**Earth Surface Processes and Landforms**
*Earth Surf. Process. Landforms* **33**, 1892–1911 (2008)
Published online in Wiley InterScience
(www.interscience.wiley.com) **DOI:** 10.1002/esp.1734

# Numerical simulation of two East Asian dust storms in spring 2006

Jianhua Sun[1]* and Linna Zhao[2]
[1] *Institute of Atmospheric Physics, Chinese Academy of Sciences, Beijing, China 100029*
[2] *National Meteorological Center, China Meteorological Administration, Beijing, China 100081*

**Correspondence to: Jianhua Sun, Institute of Atmospheric Physics, Chinese Academy of Sciences, Beijing, China 100029. E-mail: sji@mail.iap.ac.cn*

Received 18 May 2007;
Revised 29 November 2007;
Accepted 30 November 2007

## Abstract

**In this study we focus the investigation on two dust-storm events that occurred in spring 2006 over northern China. The first event occurred on 9–11 April and was the most severe in spring 2006 (Case I), whereas the second event occurred on 16–17 April (Case II) and caused widespread dust deposition in northern China, especially in the vicinity of Beijing. The weather systems that generated these dust storms were cold fronts associated with Mongolia cyclones. These events are simulated using a dust-storm model developed at the Institute of Atmospheric Physics, Beijing. The simulated dust concentrations are found to agree well with the synoptic records and satellite images. The simulated results are also compared with $PM_{10}$ measurements at the several stations. The comparisons show that the model can predict the rate of dust emission and airborne dust concentration reasonably well. The numerical results are used to analyse the dust emission, transport and deposition associated with the dust storms. The different characteristics of the weather systems that generated the two dust storms are examined in detail. Copyright © 2008 John Wiley & Sons, Ltd.**

**Keywords: dust storms; dust emission; deposition; dust transport; dust model**

## Introduction

Dust storms frequently occur in Mongolia and in the northern parts of China, especially in the spring season when strong winds lift large quantities of dust particles into the atmosphere and carry them downstream. The dust storms in this region are referred to as East Asian dust storms. In the 1990s, East Asian dust storms were relatively less frequent, but have been very active again since the turn of the century. High dust-storm frequencies have been recorded in 2000, 2001 and 2002 (Shao *et al.*, 2002, 2003; Zhou *et al.*, 2002; Sun *et al.*, 2006; Zhao and Zhao, 2006). In the spring of 2006, 18 dust events were identified by the China National Meteorological Centre, including five severe dust storms, six dust storms and seven blowing dust events. The frequency of dust events in 2006 is the highest since 2000.

The quantitative prediction of dust storms is impossible unless the entire dust cycle, consisting of dust emission, transport and deposition, can be correctly predicted. In recent years, dust emission schemes have been developed that account reasonably well for the impacts of atmospheric forcing and land-surface properties on dust emission (Marticorena and Bergametti, 1995; Shao *et al.*, 1996; Marticorena *et al.*, 1997; Shao, 2001, 2004). Duststorm modelling systems have been successfully implemented by a number of research groups (Shao and Leslie, 1997; Wang *et al.*, 2000; Uno *et al.*, 2001; Gong *et al.*, 2003). An integrated system was applied to real-time dust-storm prediction in the National Meteorological Centre of China (Shao *et al.*, 2003).

At the Institute of Atmospheric Physics of the Chinese Academy of Sciences, jointly with the China National Meteorological Centre, a new integrated dust-storm prediction system has been developed for the operational prediction of dust storms in East Asia (hereafter IAPS1.0, Sun *et al.*, 2003, 2006). The IAPS1.0 couples the Pennsylvania State/National Center for Atmospheric Research MM5 model (Grell *et al.*, 1994), a dust model and a geographical information system (GIS) database. The dust emission scheme used in IAPS1.0 was as described in Shao (2001, 2004). The system has been further improved by Lei *et al.* (2005) by replacing the Oregan State University (OSU) land-surface model with the NOAH land-surface model in MM5. The new system is referred to as IAPS2.0.

In the following section the general characteristics of dust activities in East Asia in spring 2006 are presented and the synoptic systems that generated the two severe dust storms are described. A description of IAPS2.0, the simulation results, the verifications against the observations and the analyses of dust emission, transportation and deposition are presented in the penultimate section, followed by the conclusions.

## Dust Activities in Spring 2006

### Basic characteristics of dust weather

Dust events are classified into four categories: dust-in-suspension, blowing dust, dust storm and severe dust storm according to the WMO GTS (World Meteorological Organization, Global Telecommunication System) code. The definitions of these classes are made according to horizontal visibility. In this section, three-hourly surface observations are used to analyse the features of East Asian dust activities in spring 2006.

Dust weather records are used to define the intensity and extent of the dust events. The domain of analysis is confined to 30–60° N and 90–140° E, which includes Mongolia, the northern part of China, the Korean Peninsula and Japan. All dust events are divided into two categories: weak dust events including dust-in-suspension and blowing dust, and strong dust events including dust storm and severe dust storm. We denote the total number of stations at which weak dust events were reported as $N_w$ and that of stations at which strong dust events were reported as $N_s$. Figure 1 shows the time series of $N_w$ and $N_s$ for the period March to May 2006. As can be seen, dust was widespread in March and April, with the strongest events being those that occurred on 9–11 March, 5–7 April, 9–11 April and 16–17 April. The dust events in 2006 can be grouped into 18 episodes, including five severe dust storms and six dust storms (Table I). All these episodes were caused by strong cold-air outbreaks associated with Mongolia cyclones or cold fronts. On the basis of its duration and extension, the event of 9–11 April was considered to be the strongest in spring 2006. Five dust storms occurred in May, but they were weaker than those that occurred in March and April (Figure 1a). Dust episodes were almost continuous from early March to middle April (Figure 1b). Dust events from the last 10 days of April to May are generally weaker.

Further, the frequency of strong dust events, $f_s$, and that of weak dust events, $f_w$, are calculated for northern China, as shown in Figure 2. The highest value of $f_s$ is found to occur in Inner Mongolia and the Tarim Basin. For the Tarim Basin, $f_s$ is generally <5; for Inner Mongolia, it is generally >5, reaching 10 at some stations (Figure 2a). In comparison with $f_s$, $f_w$ is higher. Weak dust events affect much of northern China, except Jilin, Heilongjiang and north Xinjiang. There are profound differences between the distributions of $f_s$ and $f_w$. Strong dust events occur more frequently over the Gobi Desert in Mongolia and Inner Mongolia. The frequency of strong dust events is relatively low in other areas. Strong dust events occur occasionally in the Tarim Basin, where weak dust events are most frequent. The seasonal variation studies of dust activities in the Tarim Basin indicated that blowing dust and dust-in-suspension events occurred throughout the year, and dust storm and severe dust storms events occur frequently in the spring (Shao and Dong, 2006).

Although 18 episodes occurred during spring 2006, only the 9–11 April (Case I) and 16–17 April (Case II) episodes will be studied in this paper.

**Table I.** Major dust storm events over northern part of China in Spring 2006

| Date | Class | Weather system | Date | Class | Weather system |
|---|---|---|---|---|---|
| 9–12 March | SDS | MC/CF | 21–23 April | DS | MC/CF |
| 16–17 March | BDS | MC/CF | 24–25 April | BDS | MC/CF |
| 24–25 March | BDS | MC/CF | 28–30 April | BDS | MC/CF |
| 26–27 March | SDS | MC/CF | 6 May | DS | MC/CF |
| 30–31 March | BDS | MC/CF | 8 May | BDS | CF |
| 5–7 April | SDS | MC/CF | 10–11 May | DS | CF |
| 8 April | DS | MC/CF | 15–18 May | DS | MC/CF |
| 9–11 April | SDS | MC/CF | 19–20 May | DS | CF |
| 16–18 April | SDS | MC/CF | 29–30 May | DS | MC/CF |

SDS, severe dust storm; DS, dust storm; BDS, blowing dust event; MC, Mongolia cyclone; CF, cold front.



DOI: 10.1002/esp

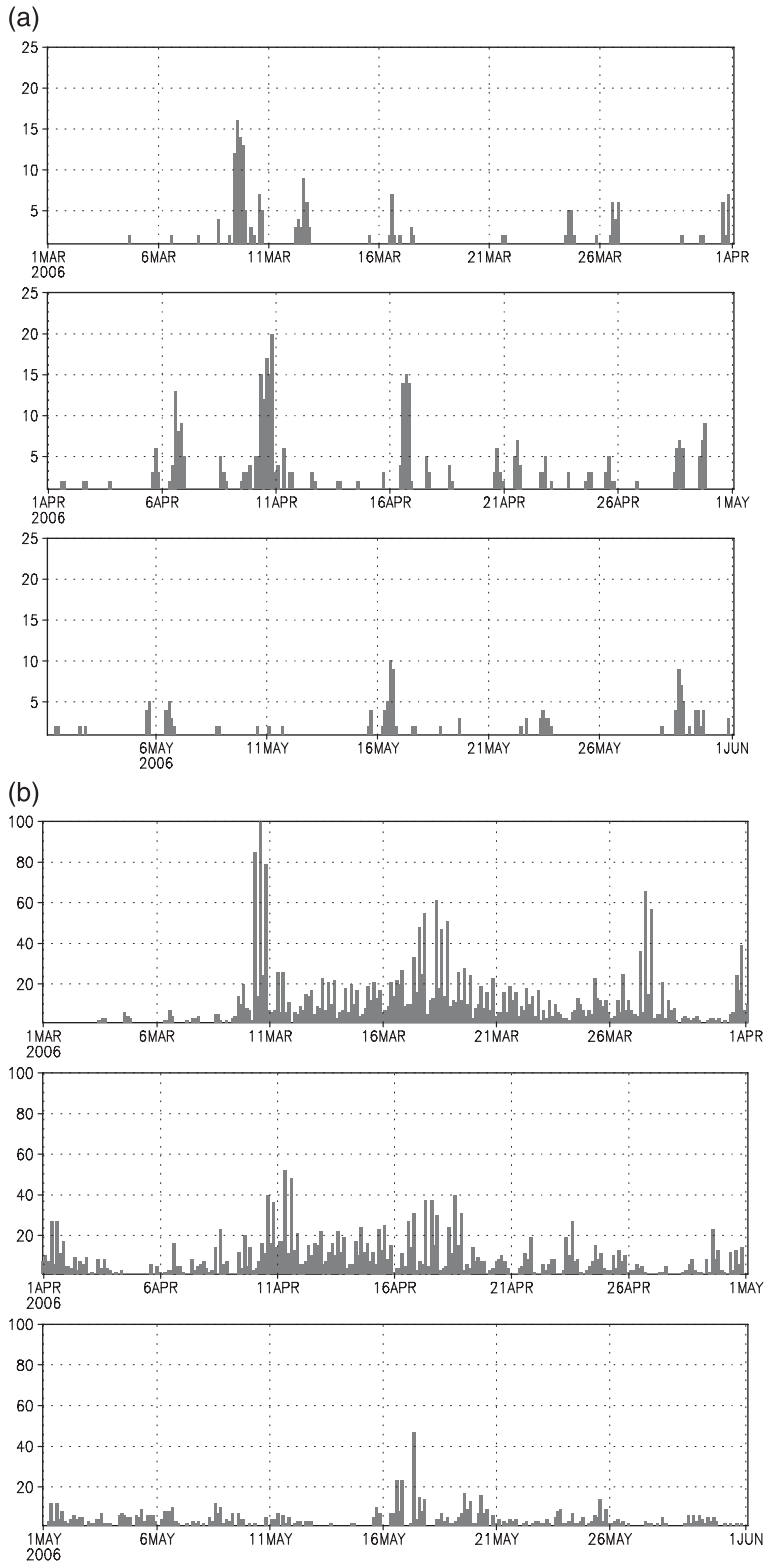


**Figure 1.** (a) The daily number of stations at which dust storms and severe dust storms are observed in the study domain for March, April and May 2006. (b) As (a), but for dust-in-suspension and blowing dust events.



DOI: 10.1002/esp

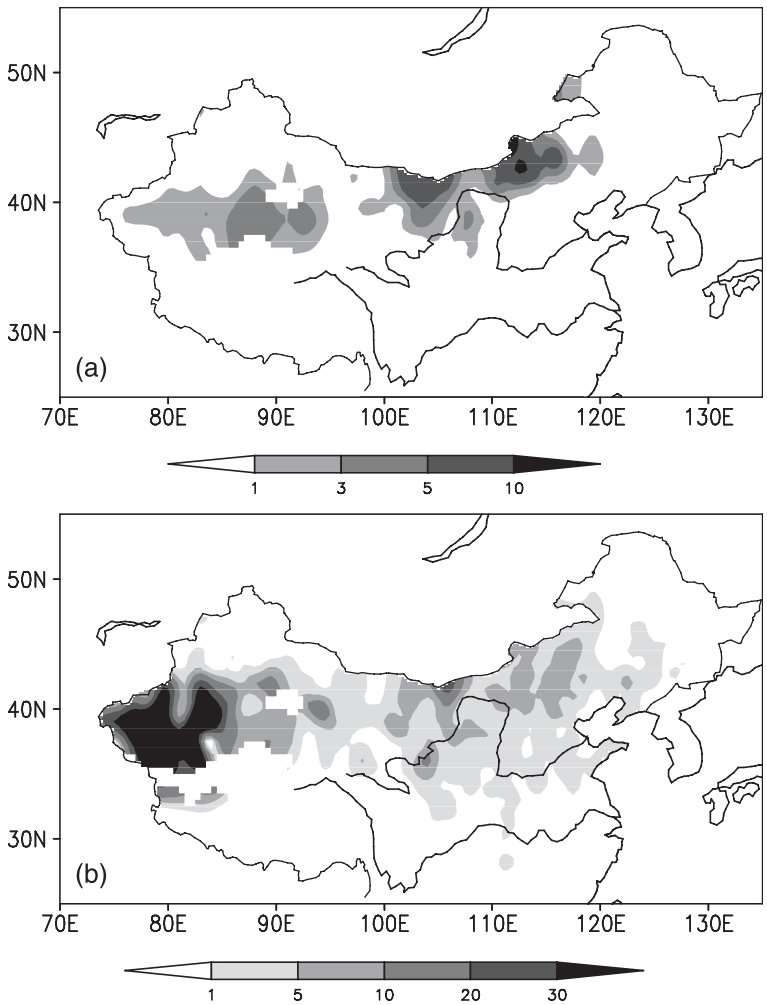


**Figure 2.** (a) Frequency of strong dust events and (b) weak dust events for March, April and May 2006, as observed by the Chinese Meteorological Network.

## The 9–11 April event (Case I)

The 9–11 April dust storm, which originated in the Tulufan Basin, was the strongest dust event in the past 22 years. It resulted in the loss of eight lives and caused severe damage to the passenger train on route from Urumqi to Beijing on the night of 9 April 2006, as well as 11 traffic accidents on the highways in Inner Mongolia due to very low visibility. Figure 3a and b shows the fields of geo-potential height and temperature at 500 hPa for the event. From 9 to 11 April, dust storms occurred in northwestern China and northern China, but the most severe storm was observed during the daytime of 10 April. A trough at 500 hPa located at 60° E at 0000 UTC 8 April (not shown) moved to the China–Mongolia border at 0000 UTC 9 April (Figure 3a). The trough split into two parts in the next two days. One part moved rapidly eastward, producing dust weather in northern China and the other part developed southward, causing dust weather in Pakistan and northern India (not shown). Accompanying the development of the trough, a cyclone formed over the Mongolia Plateau in the lower troposphere (not shown) on 9 April, which then intensified and moved eastward in the next two days. Generally, strong westerly or northwesterly surface winds, reaching up to 20 m $s^{-1}$, occurred over Mongolia and Inner Mongolia, causing strong dust emission in the cold regime of the cyclone. Strong winds also occurred in the Tulufan Basin, probably due to the local topographic forcing. In the Tarim Basin, dust storms were observed.

Although dust storms occurred both in the Tarim Basin and over the Gobi in this dust episode, the weather systems related to the dust storms in the two regions were quite different. Dust storms over the Gobi may be caused directly by



DOI: 10.1002/esp

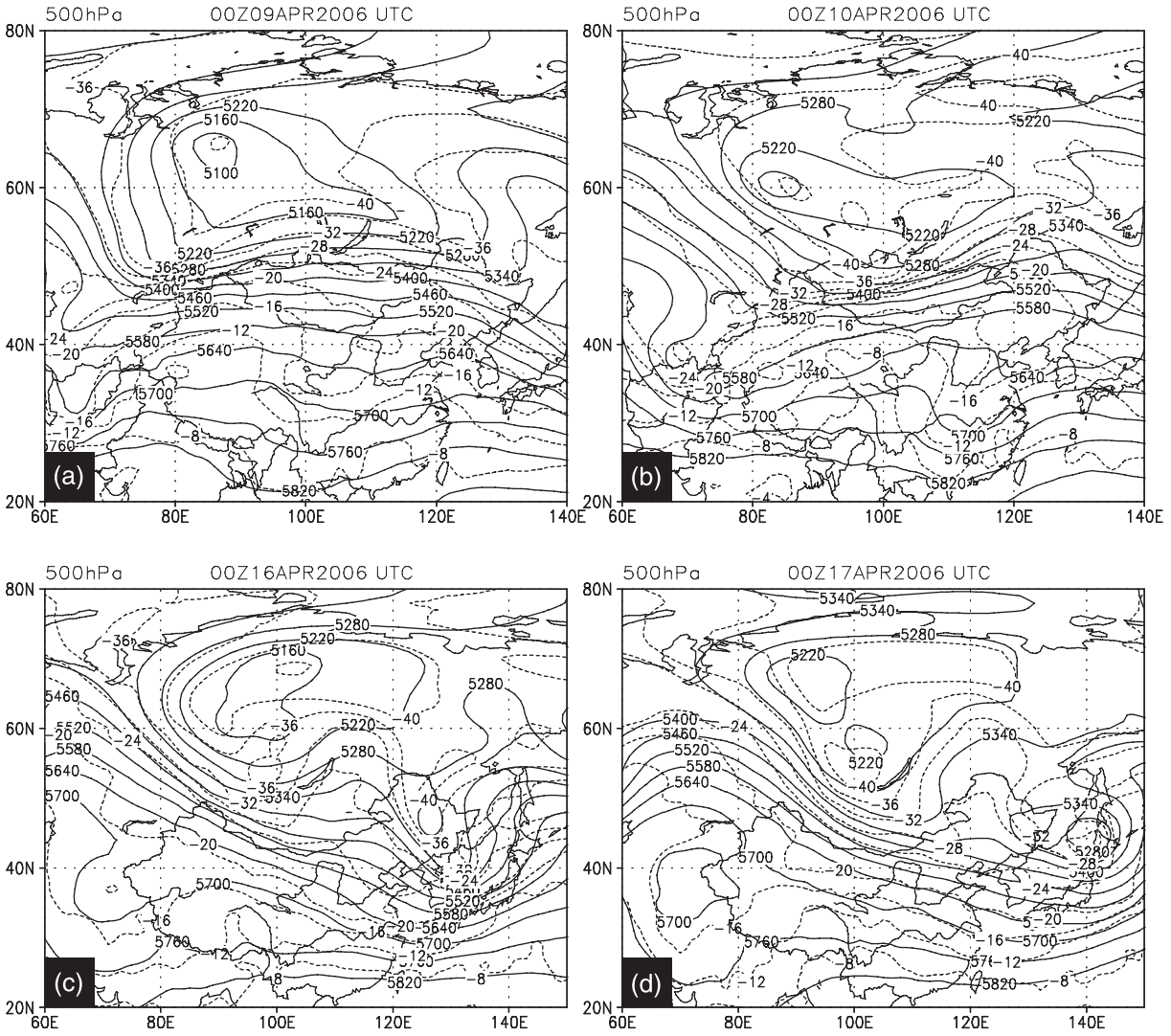


**Figure 3.** Geo-potential height (gpm: solid line) and temperature (°C: dashed line) at 500 hPa on April 2006: (a) 0000 UTC 09 April; (b) 0000 UTC 10 April; (c) 0000 UTC 16 April; (d) 0000 UTC 17 April.

the strong winds of the cyclone. In the Tarim Basin, dust emission is caused by four mechanisms: strong northeasterly airflow from the eastern inlet; strong northerly airflow climbing over the Tianshan Mountains; local wind and convective system (Shao and Dong, 2006). Shao and Wang (2003) suggested that strong northeasterly winds often affect the eastern and southeastern parts of the Tarim Basin and generate dust storms there. For the present case, dust emission in the Tarim Basin was also generated by the strong northeasterly airflow. The topography of the Tarim Basin plays a significant role in the formation of the easterly wind, as will be discussed in the next section.

## The 16–17 April event (Case II)

During this event, strong dust deposition occurred in northern China, especially in Beijing on 16–17 April. Although both Case I and Case II were associated with Mongolian cyclones, the dust-affected areas were different because the cyclones propagated along different paths.

The 16–17 April 2006 event was also produced by a Mongolian cyclone. Associated with this low pressure system was a cold front in the lower troposphere and a cut-off low aloft (Figure 3c and d). The track of this cyclone was similar to that for Case I, but it was somewhat to the northeast and did not affect the Tarim Basin. A deep trough was



DOI: 10.1002/esp

propagating eastwards from 80° E at 0000 UTC 15 April to the coastal region at 0000 UTC April 18. A trough was located to the north of Baikal Lake at 0000 UTC 16 April (Figure 3c). In the next two days, this trough moved northeastward, intensified and extended into Mongolia and Inner Mongolia. At the same time, a trough was located over Afghanistan, Pakistan and northern India, which generated dust weather there (not shown). Accompanying the eastward propagation of the trough, a cyclone formed over eastern Mongolia in the lower troposphere (not shown). The centre of cyclone was located at the Mongolia–China border. A very strong northwesterly wind with velocity exceeding 20 m $s^{-1}$ resulted in blowing dust and a dust storm over southern Mongolia, Inner Mongolia and other parts of northern China (not shown). The dust weather was also observed in the southeasterly wind area ahead of the cold front.

## The Dust Model and the Simulations

### The Integrated Dust Modelling System

The first version of the Integrated Dust Modelling System, IAPS1.0 has been described in Sun *et al.* (2003, 2006). Here, we shall focus on its second version, IAPS2.0. The structure of IAPS2.0 is as illustrated in Figure 4. It consists of a GIS database, a preprocessor, a regional weather model (MM5V3.7, the PSU/NCAR mesoscale model together with the NOAH land-surface model), a dust emission model and a dust transport model. The weather model, dust emission model and dust transport model are numerically integrated successively for each time-step. The dust emission model is coupled with the NCEP MRF (National Center for Environmental Prediction, Medium-Range Forecast model) high resolution PBL (Planetary Boundary Layer) scheme (Hong and Pan, 1996) and the NOAH land-surface model. The MM5 weather model provides the atmospheric data to force the dust emission and transport models. For each time-step, friction velocity from the PBL scheme and soil moisture from the land-surface scheme are passed to the dust emission model for the calculation of the dust emission rates for different particle-size groups. The dust emission rates and atmospheric variables (e.g. wind field and turbulence parameters) are then passed to the dust transport model for computing instantaneous grid-mean dust concentration. The parameters of soil type and vegetation categories, required by the dust emission scheme, are prepared by a GIS preprocessor.

The land-surface model is an important scheme which relates atmospheric simulation to dust emission modelling. In IAPS1.0, the Oregon State University/NCEP Eta Land-Surface Model (OSULSM) was used in MM5 (Chen and Dudhia, 2001a,b). In IAPS2.0, OSULSM is replaced with the NOAH LSM. The latter (Chen and Dudhia, 2001a,b) is

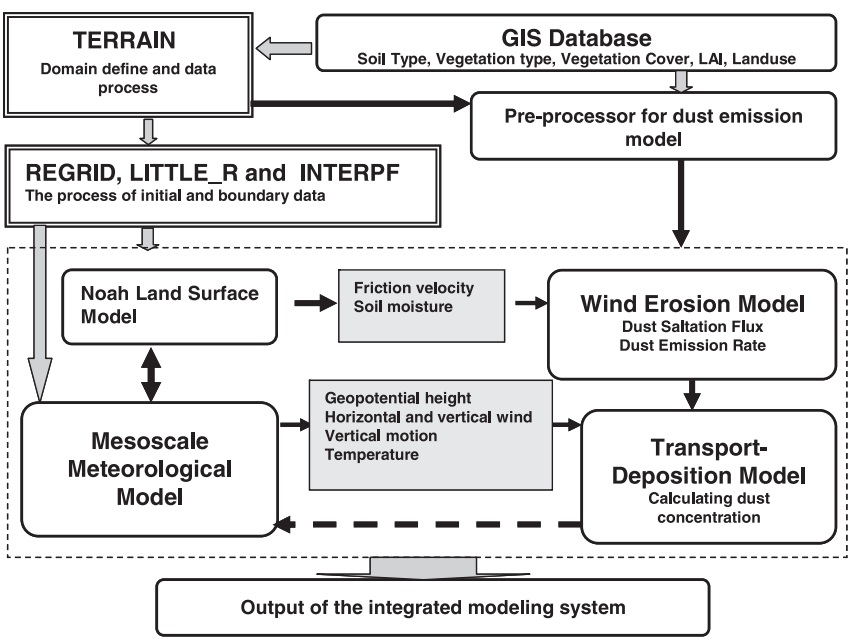


**Figure 4.** Framework of the Institute of Atmospheric Physics (Beijing) integrated dust-storm modelling and prediction system IAPS2.0.



DOI: 10.1002/esp

**Table II.** Differences of parameterization of physical processes between NOAH and OSU land surface schemes

| Physical processes | NOAH LSM | OSU LSM | Reference |
|---|---|---|---|
| Frozen soil physics | Yes | No | Koren *et al.* (1999) |
| Fractional snow cover | Yes | No | Koren *et al.* (1999) |
| Time-varying snow density | Yes | No | Koren *et al.* (1999) |
| Roughness length calculation over snow-covered area | New | Old | Chen *et al.* (1997) |
| Heat flux under snow pack | Yes | No | Lunardini (1981) |
| Snow albedo calculation | New | Old | Robinson and Kukla (1985) |
| New soil thermal conductivity | New | Old | Peters-Lidard *et al.* (1998) |
| Vegetation reduction of thermal condition | Yes | No | Peters-Lidard *et al.* (1998) |
| Rooting depth dependent on vegetation types | Yes | No | Peters-Lidard *et al.* (1998) |

based on coupling of the diurnally dependent Penman potential evaporation approach of Mahrt and Ek (1984), the multilayer soil model of Mahrt and Pan (1984), and the primitive canopy model of Pan and Mahrt (1987). It has been extended by Chen *et al.* (1996) to include the modestly complex canopy resistance approach of Jacquemin and Noilhan (1990) and by Koren *et al.* (1999) to include frozen ground physics. A LSM is used to predict soil moisture and temperature in four layers with thicknesses from top to bottom of 10, 30, 60 and 100 cm, as well as canopy moisture and water-equivalent snow depth. The LSM uses soil and vegetation types in handling evapotranspiration. Vegetation parameters (e.g., roughness length and albedo) depend on vegetation type. The NOAH LSM can optionally use satellite-derived climatological albedo, instead of relying on albedo–land-use empirical relationships. The main differences between OSU and NOAH LSMs are listed in Table II. More details on this LSM can be found in the related references (Chen and Dudhia, 2001a,b). It is coupled with MM5 through the Medium-Range Forecast (MRF) PBL (Hong and Pan, 1996) schemes.

The NOAH LSM is coupled to the MM5 model through the lowest atmospheric level, which is also referred to as the surface layer. A surface-layer parameterization provides the surface (bulk) exchange coefficients for momentum, heat and water vapour to determine the fluxes of these quantities at the land surface. The surface-layer parameterization bases its surface flux calculations on the similarity theory, using a stability-dependent function and roughness length to determine the surface exchange coefficients for heat and moisture. These exchange coefficients are passed to the LSM from the PBL scheme, together with surface radiation forcing terms and precipitation rate. The LSM routine returns to the PBL scheme the surface heat and moisture fluxes for calculation of the boundary layer flux convergence, which contributes to atmospheric temperature and moisture tendencies.

Both IAPS2.0 and IAPS1.0 have been used to simulate East Asian dust storms that occurred in spring 2002 (Lei *et al.*, 2005). Their results show that the simulated dust-affected regions by IAPS2.0 agree quite well with the synoptic observations, whereas those by IAPS1.0 are generally stronger and larger than the observations. For example, for the cases of 19–21 March and 5–9 April 2002, the simulation dust area over northwestern China by IAPS1.0 is stronger and larger than observation. The simulation dust area by IAPS2.0 is significantly smaller than that by IAPS1.0, at the same time, the intensity of dust concentration by IAPS2.0 is weaker than that by IAPS1.0. Further analyses suggest that the simulation of soil moisture by IAPS2.0 is wetter than that by IAPS1.0 for most of the simulation domain. It is reasonable to suggest that the improved simulations of soil moisture by using IAPS2.0 would result in improved estimates of the wind erosion threshold friction velocity.

## Model configuration and initialization

The simulation domain is centred at (40° N, 95° E) for Case I and at (40° N, 105° E) for Case II, which covers Mongolia, China, the Korean Peninsula and Japan. It consists of $120 \times 150$ grid points with a horizontal resolution of 45 km. An additional domain centred at (30° N, 88° E) is prepared for Case I. This domain has $142 \times 163$ grid points with a horizontal resolution of 15 km. The model top is located at 50 hPa and has 31 vertical sigma levels. The microphysics for explicit moisture processes is treated using the mixed-phase microphysics scheme of Reisner *et al.* (1998). The cumulus parameterization scheme of Grell *et al.* (1991) is used for subgrid-scale convection. The NCEP MRF high-resolution PBL scheme (Hong and Pan, 1996) is adopted to calculate the turbulent fluxes in the PBL.

Six-hourly global analyses data, with a $1° \times 1°$ resolution from the NCEP are interpolated horizontally onto the model grid points, and then from pressure levels onto the model $\sigma$ levels. The dust concentration of each particle size group is given as zero initially. The numerical integrations start at 0000 UTC 09 April and 0000 UTC 16 April 2006,



DOI: 10.1002/esp

and end at 0000 UTC 11 April and 0000 UTC 19 April 2006, respectively. The time-dependent, lateral boundary conditions are provided by interpolating the six-hourly observational analyses linearly in time. For soil moisture initialization, the volumetric soil moisture fields of NCEP reanalysis for four soil layers (0–10, 10–40, 40–100 and 100–200 cm) are interpolated to the four soil layers for the MM5–LSM.

## Validation of model simulation

We have verified the simulation results using weather station observations, satellite images and $PM_{10}$ observations.

*The 9–11 April 2006 event (Case I).* First, the simulated near-surface dust concentration is compared with the visibility data obtained at the weather stations. The visibility is converted to dust concentration using an empirical relationship given in Shao *et al.* (2003). In Figure 5, the simulated and visibility-derived dust concentrations are compared for the time period from 0300 UTC 09 April to 2100 UTC 10 April 2006. The visibility-derived concentrations below 1 mg $m^{-3}$ are not shown in Figure 5. The figure shows that simulated and observed dust patterns are in general agreement. It is found that dust storms first developed in the Tarim Basin and then over the Gobi Desert. In the subsequent hours, the severe dust storm region extended both eastward and westward. On 9 April 2006, the dust-affected area was northwestern China. On 10 April, the dust storm moved eastwards, spreading widely and affecting Inner Mongolia, Shanxi and Hebei. Severe dust storms occurred in the vicinity of the sandy land surface. Both the simulation and observation show that a 3500-km-long dust band extended from northeastern China to northwestern China. Dust intensity on 10 April was stronger than on 09 April, with the dust-affected area covering almost the entire northern part of China. It can be seen from the evolution of the event, that the main dust sources are the Gobi Desert in Mongolia and the sandy deserts in Xinjiang and Inner Mongolia, China.

The satellite images of the dust storm from NOAA16/17, TERRA/MODIS (Moderate Resolution Imaging Spectro-Radiaometer) and FY (FengYun)-1D satellites, prepared by the National Satellite Meteorological Centre of the China Meteorological Administration (NSMC/CMA) are also used for comparison. The techniques used to identify dust clouds from satellite imagery have been described in Shao and Dong (2006) and Zhang *et al.* (2006). A comparison of the satellite images and the simulated dust concentration fields shows that the simulated dust-affected regions in Inner Mongolia and Mongolia agree well with the observation (not shown). The satellite image for 1123 UTC 09 April indicates that the dust cloud arrived at northeastern China and Hebei Province, but the simulated dust cloud arrived there after 0600 UTC 10 April, later than observed (Figure 5).

Two centres of high dust concentration are found to be located in the Tarim and the Tulufan Basin (Figure 5). For the dust event, the weather pattern in the Tarim Basin was substantially different to those over the Gobi Desert. The Tarim Basin is adjacent to the Tibetan Plateau and surrounded by mountains, except for the eastern part leading into the Hexi Corridor. The topography surrounding the Tarim Basin and the Tulufan Basin for Domain 2 is shown in Figure 6. The numerical simulation with the 15 km resolution, the Tianshan Mountains and the topography surrounding the Tulufan Basin are well resolved. The Taklimakan Desert is 1400 km long in the east–west direction and 550 km wide in the south–north direction. We now use the hourly model outputs with the 15 km horizontal resolution to investigate the relationship between the mesoscale system and dust emission.

The topography surrounding the Tarim Basin significantly affects the local circulation. Seino *et al.* (2005) found that strong surface winds in the Tarim Basin are associated with three types of the mesoscale flow: a westerly flow from over the Pamir Plateau; a northerly flow associated with a severe downslope wind over the Tianshan Mountains; and an easterly flow extending from the eastern end of the basin following the cold air outbreak to the north of the Tianshan Mountains. Our simulation indicates that the dust events in the Tarim Basin on 9 April were related to the strong wind associated with the low-pressure system, but those on 10 April were related to the subsequent high-pressure system.

At the beginning of the simulation, a southerly wind and a westerly wind were influencing the southern and eastern part of the Tarim Basin (Figure 7a). Dust emission occurred only in the southern part. In the following hours, with the eastward propagation of the Mongolian cyclone, cold air intensified to the north of the Tianshan Mountains. The northerly downslope wind over the Tianshan Mountains gradually spread into the basin. At the same time, an easterly flow invaded into the Tarim Basin from the eastern inlet (Figure 7b–d). The severe northeasterly resulted in strong dust emission in the Tulufan Basin and the Tarim Basin. The simulated dust concentration over this area reached 20 mg $m^{-3}$ (Figure 5). In the present case, the local circulation in the Tarim Basin differs from the three flow types identified by Seino *et al.* (2005).

The vertical cross-section along 85° N shows that two vertical circulations exist in the middle troposphere over the Tarim Basin, the upward motion was over the middle part of the Tarim Basin, and two downdrafts were over the north rim of Tibet and the Tianshan Mountains (Figure 8a and b) at the earlier stage of the event. The vertical circulation over the Tarim Basin changed significantly in the subsequent hours. The two vertical circulations were replaced by one vertical circulation, which was composed of a northerly wind in the lower troposphere and a southerly wind in the



DOI: 10.1002/esp

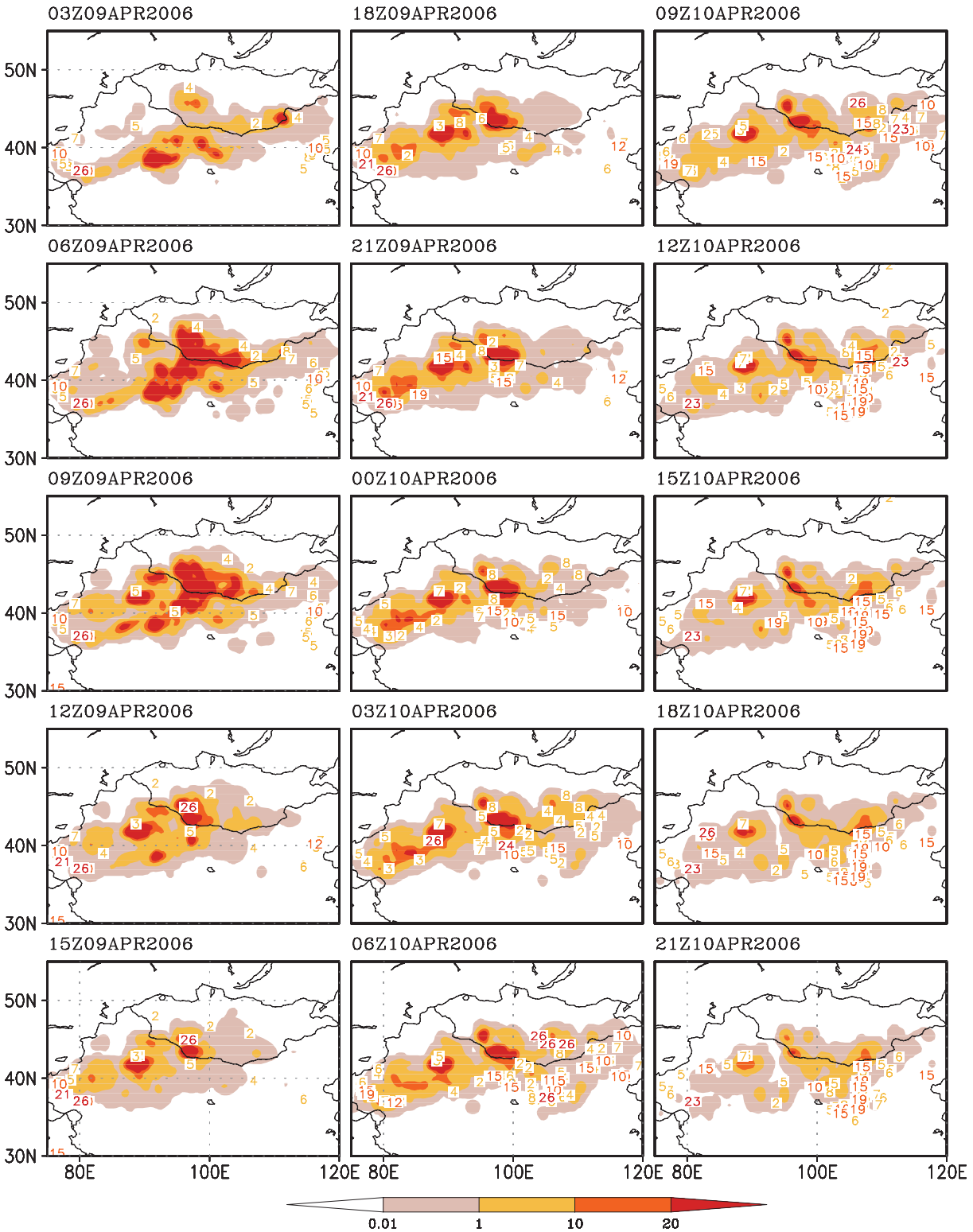


**Figure 5.** A composition of simulated surface dust concentration (shaded: mg $m^{-3}$) and the visibility-derived near-surface dust concentration (numbers) from 0300 UTC 9 to 2100 UTC 11 April 2006.




DOI: 10.1002/esp

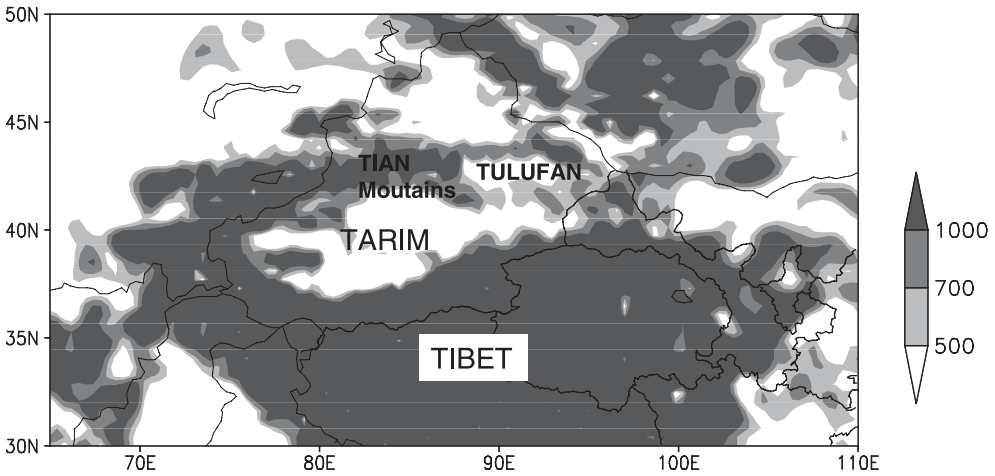


**Figure 6.** Topography around the Tarim Basin (m). Areas with elevation higher than 500 m are shaded.

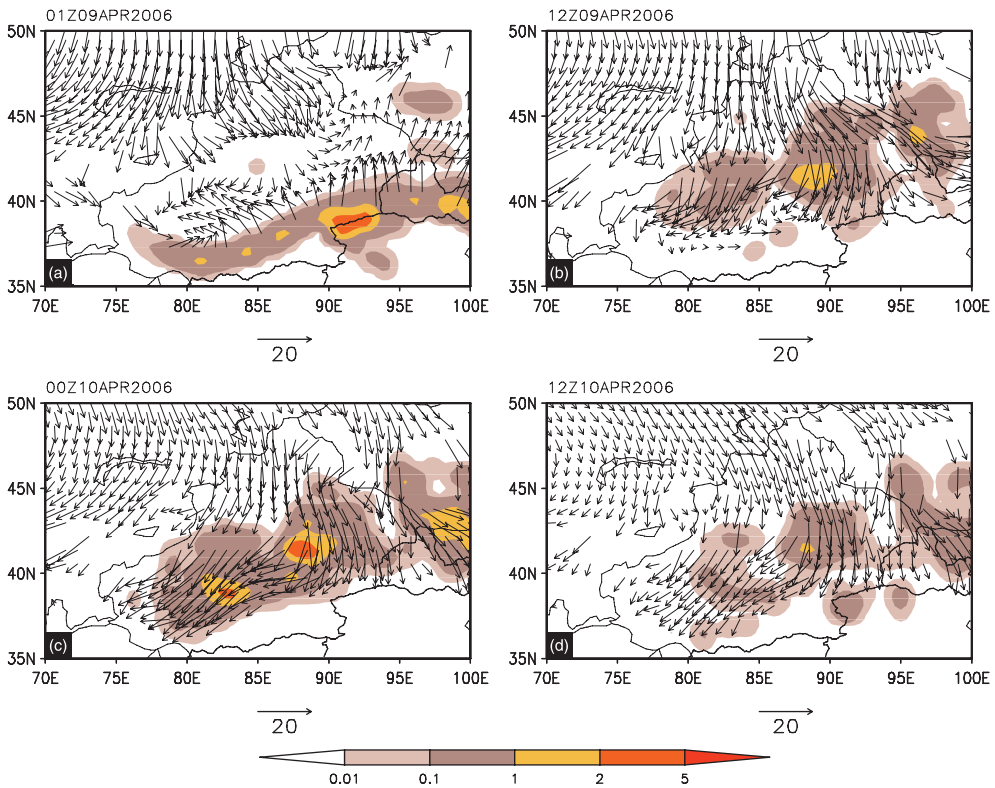


**Figure 7.** The dust emission rate (shaded: mg $m^{-2}$ $s^{-1}$) and wind vectors at 850 hPa, (a) 0100 UTC 9 April, (b) 1200 UTC 9 April, (c) 0000 UTC 10 April and (d) 1200 UTC 10 April.

middle troposphere. Dust emission was mainly generated by the northerly wind and then transported to the northern rim of Tibet plateau (Figure 8c–e). The dust was then further transported northward by the southerly wind in the middle troposphere to as far as over the Tianshan Mountains (Figure 8f–h).

*The 16–18 April 2006 event (Case II).* Similar to Figure 5, the simulated dust concentration for the 16–17 April 2006 is compared with the observations in Figure 9. In comparison to the observations, the simulated dust area was



DOI: 10.1002/esp

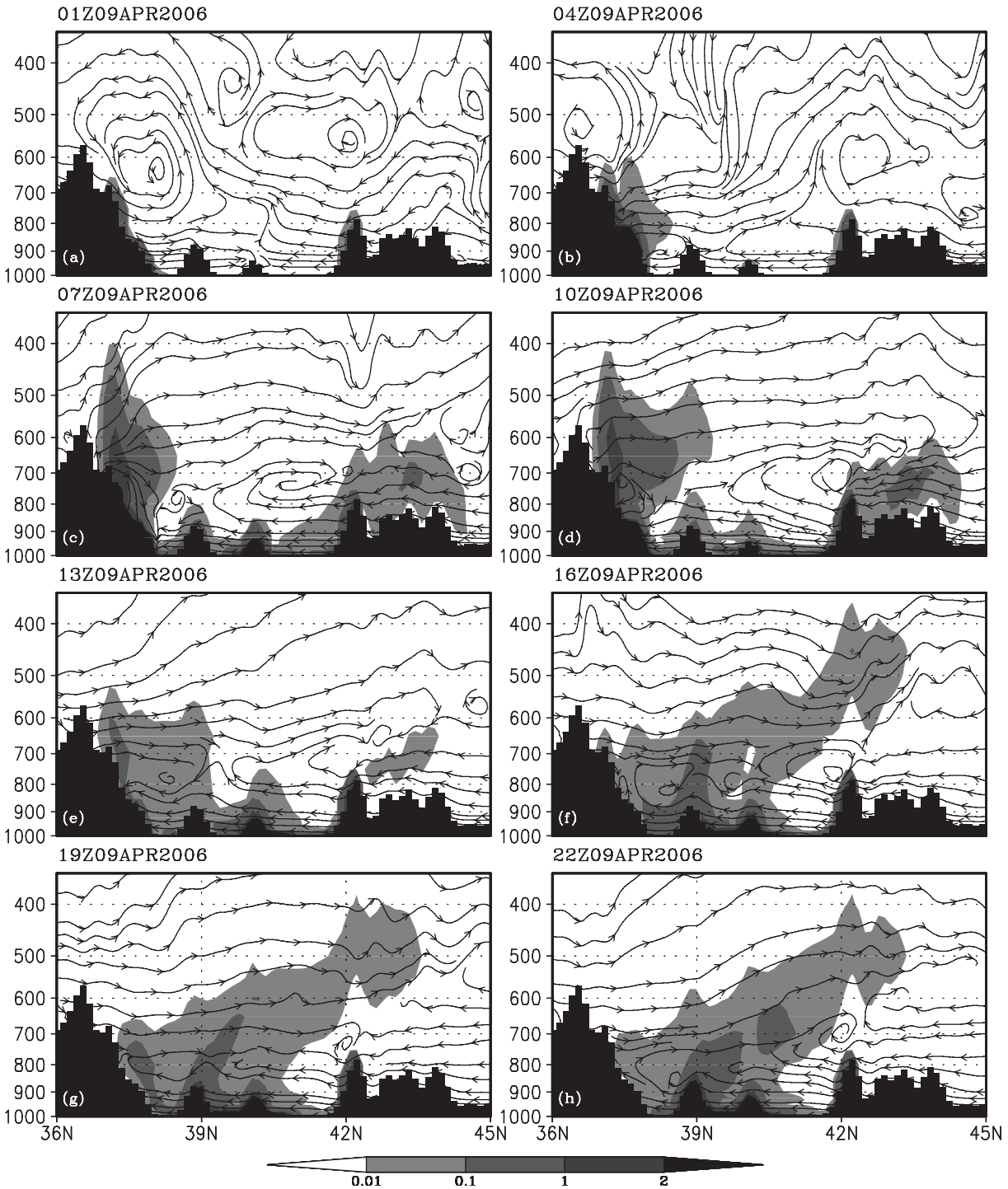


**Figure 8.** The meridional wind and vertical motion (stream line) and dust concentration (light shading: mg $m^{-3}$) for a vertical cross-section along 85° E; the dark shaded area represents the topography.



DOI: 10.1002/esp

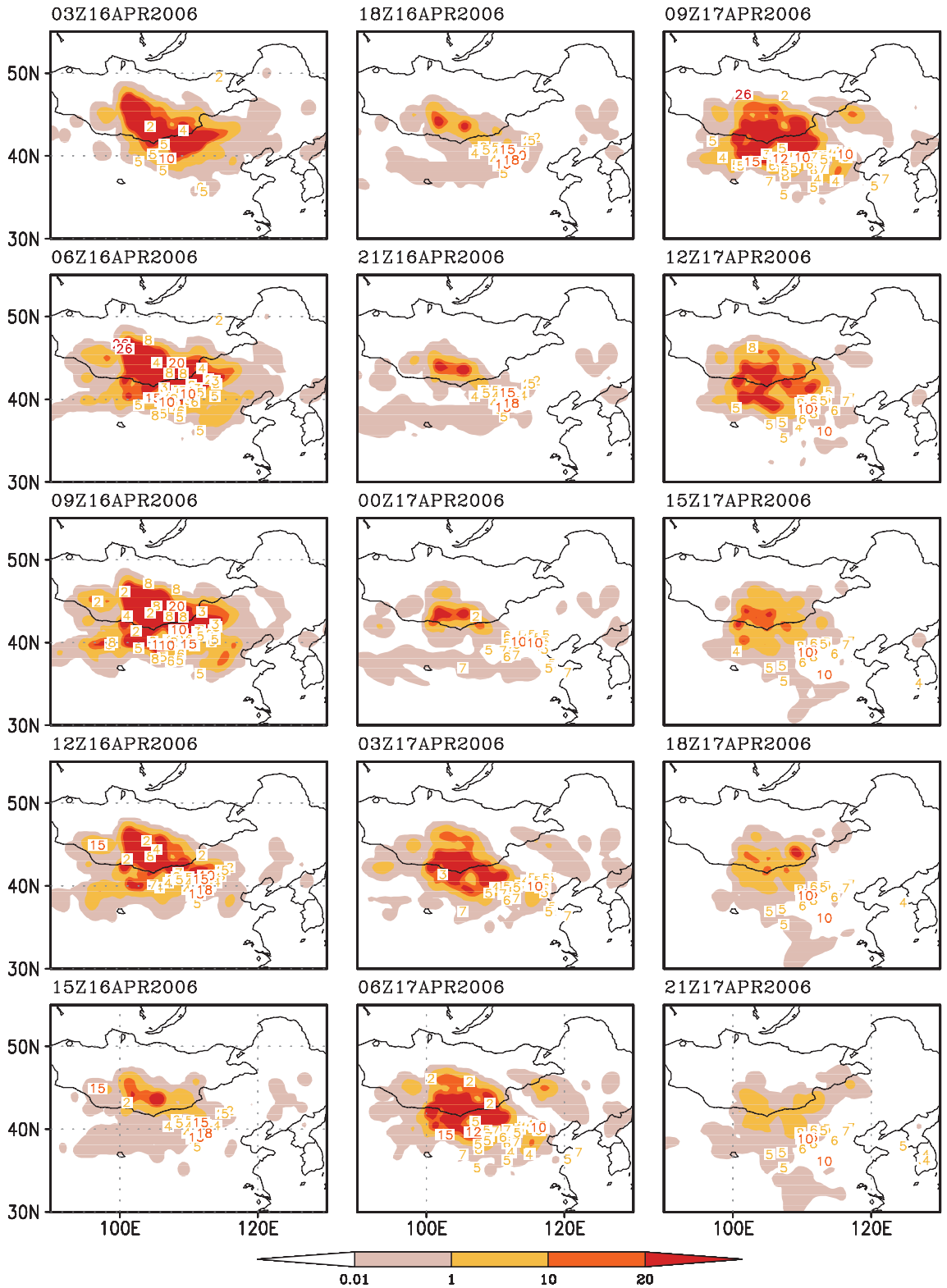


**Figure 9.** A composition of simulated surface dust concentration (shaded: mg $m^{-3}$) and the observed (numbers: mg $m^{-3}$) at the surface from 0300 UTC 16 to 2100 UTC 17 April 2006.




DOI: 10.1002/esp

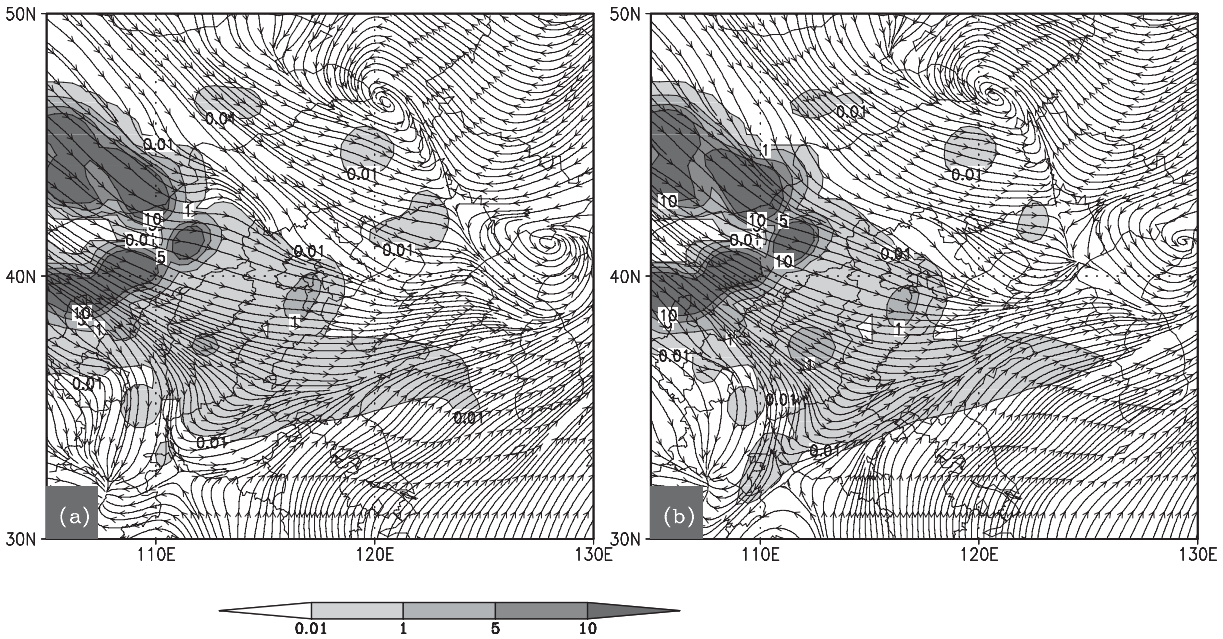


**Figure 10.** The simulated dust concentration (shaded: mg $m^{-3}$) and stream line at 850 hPa at (a) 0600 UTC 17 and (b) 0900 UTC 17 April 2006.

too much to the west and the intensity was weaker than expected. The simulation for the 16 April is better than that for the 17 April.

Severe dust storms occurred over southern Mongolia and Inner Mongolia at 0300 UTC 16 April, and dust was widespread in Inner Mongolia at 0600 and 0900 UTC 16 April. According to the observations, dust affected Shanxi and Hebei in the night of 16 April, and dust storms occurred in the northern part of Shanxi and Hebei during the daytime of 17 April. For these regions, the simulated dust intensity is weaker than the observed, whereas for southern Mongolia and west Inner Mongolia the model simulated dust intensity is stronger than observed. An analysis of the simulated weather pattern shows that the simulated strong surface northwesterly wind with a speed exceeding 12 m $s^{-1}$ was located to the northwest of the observed. The incorrect simulation of the strong northwesterly wind appears to have resulted in the incorrect prediction of the dust source region.

The observed dust-in-suspension over North China and the Korean Peninsula was not successfully simulated for 17 April (Figure 9). According to satellite images (not shown), dust was blowing to the Shandong Peninsula and Bohai Sea on the morning of 17 April, and then to South Korea in the afternoon of April 17. Although the surface dust concentration was very low on 17 April, it was transported to the Korea Peninsula at 850 hPa after 0600 UTC 17 by the southwesterly in the southeast part of cyclone (Figure 10). The strong westerly transported dust eastward in the middle and lower levels, the near-surface wind was relatively weak. In addition, the southwesterly in the warm sector of the cyclone after 0600 UTC 17 April prevented the southward transportation of dust and the transport of dust to the Korean Peninsula and Northeast China (Figure 10). To illustrate the transport process, the vertical cross-sections of meridional wind, upward motion and dust concentration are shown in Figure 11. In the western part, a northerly wind prevailed and the upward motion was weak. The height of the dust layer was confined to about 600 hPa or lower and the maximum concentration was around 500 μg $m^{-3}$. In the western part, the upward motion was weak. In the eastern part, a southerly jet (maximum speed around 12–16 m $s^{-1}$) was accompanied by a stronger upward motion in the lower troposphere. A dust cloud with relatively high concentration of about 100 μg $m^{-3}$ in the layer of 800–500 hPa was propagating eastward. This dust cloud was separated from the dust centre, which was located more to the west. This shows that during this dust event the upward motion in the southeastern section of the cyclone was responsible for the vertical transport of the dust.

It is interesting to examine why strong deposition occurred in the Beijing. The numerical simulation reveals that dust concentration below 800 hPa was quite high (>50 μg $m^{-3}$) and the dust layer extended up to 600 hPa after 1800 UTC 16 April (Figure 12b). The LiDAR observation at Bejing indicates that the aerosol layer extended to between 1 and 5 km high on 16 April 2006 (Papayannis *et al.*, 2007). The wind speed below 800 hPa was weak (Figures 12b and 13) accompanied by a downward motion (Figure 12a). The soundings at Beijing (Figure 13) show an inversion



DOI: 10.1002/esp

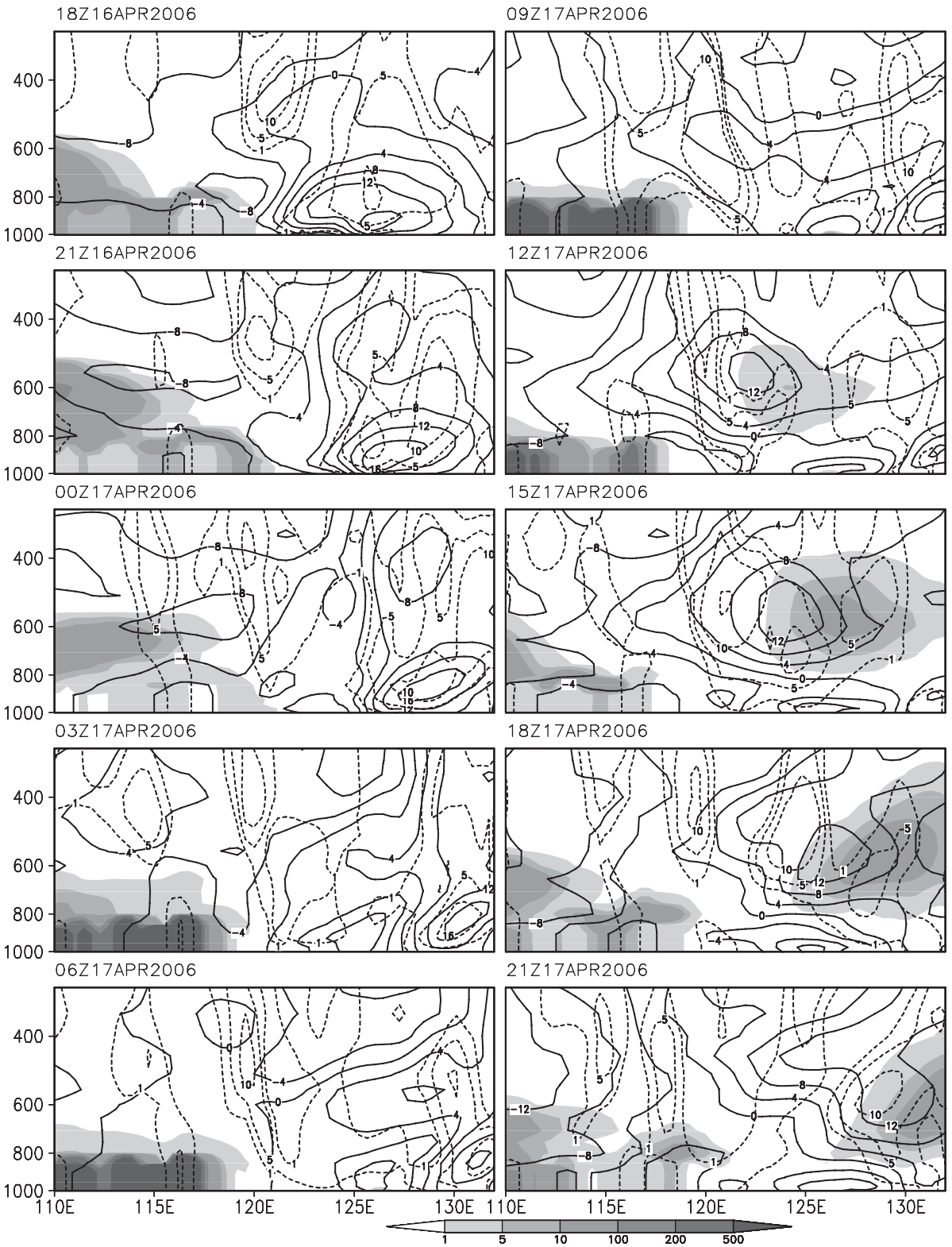


**Figure 11.** The latitude–height vertical cross-section along 39° N of simulated dust concentration (shaded: μg m$^{-3}$), meridional wind (solid line: m s$^{-1}$) and upward motion (dashed line: cm s$^{-1}$) from 1800 UTC 16 to 2100 UTC 18 April, 2006.



DOI: 10.1002/esp

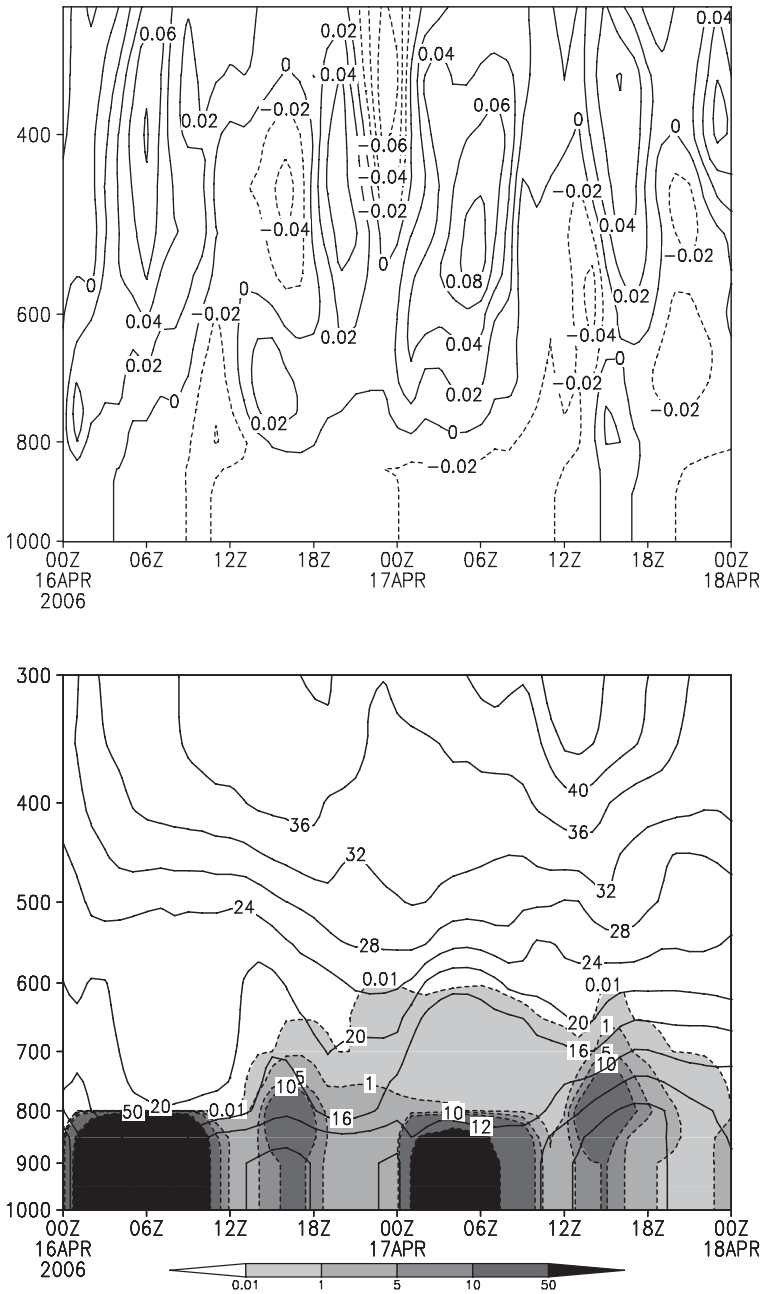


**Figure 12.** (a) The simulated vertical velocity (m $s^{-1}$), (b) wind speed (solid, m $s^{-1}$) and dust concentration (shaded: μg $m^{-3}$) at Beijing during 16–18 April 2006.

between 900 hPa and 800 hPa on 16 to 17 April. The strong dust deposition in Beijing can be attributed first to the stable stratification of the atmosphere. It can be attributed secondly to the slow propagation of the cyclone and the cold front (not shown). The cold front was slowly moving and stayed to the northwest of Beijing for 20 hours. The inversion, downward motion and the slow propagation of weather systems during the dust storm event provided favourable conditions for dust deposition.

*Verification with $PM_{10}$ measurements.* A comparison of the simulated and observed $PM_{10}$ concentrations is shown in Figure 14 for five stations in China, including Hami (93·52° E, 42·82° N, Xinjiang), Erjinaqi (101·07° E, 41·95° N, Inner Mongolia), Zhurihe (112·9° E, 42·4° N, Inner Mongolia), Beijing (116·47° E, 39·8° N) and Zhangjiakou (114·7° E,



DOI: 10.1002/esp

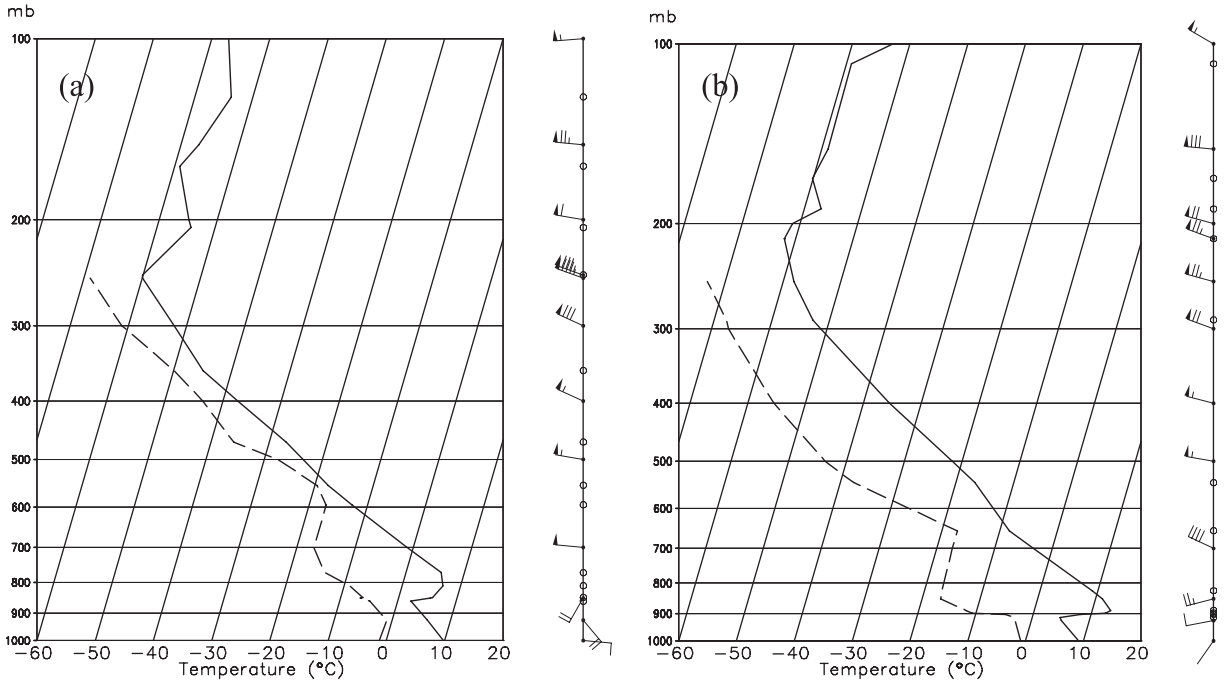


**Figure 13.** Composite sounding on skew T-log*p* diagrams at (a) 1200 UTC 16 April 2006 and (b) 0000 UTC 17 April 2006 at Beijing: temperature (bold solid line) and dew-point (bold dashed line).

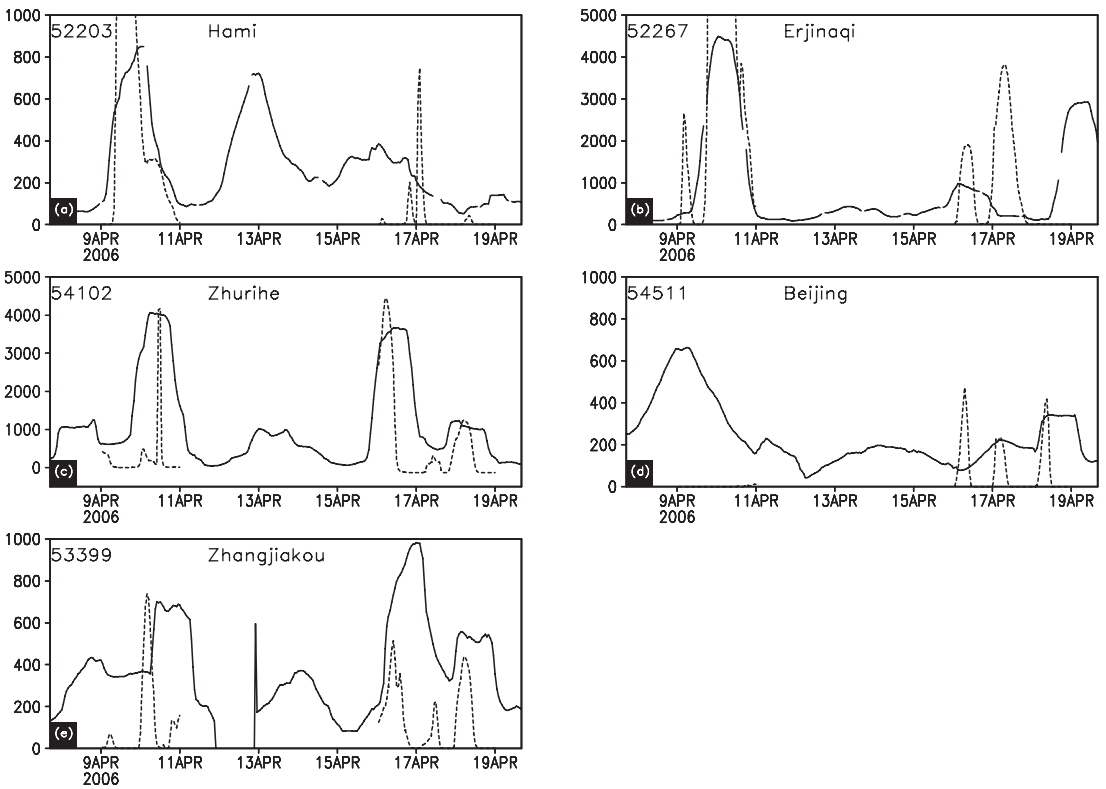


**Figure 14.** A comparison of observed $PM_{10}$ (solid line) and simulation (dashed line: $\mu g\ m^{-3}$): (a) Hami, (b) Erjinaqi, (c) Zhurihe, (d) Beijing and (e) Zhangjiakou.



DOI: 10.1002/esp

41·5° N, Hebei). The simulation results for Hami, Erjinaqi, Zhurihe and Zhangjiakou are in reasonable agreement with the $PM_{10}$ observations in Case I, except that the simulated peak values are slightly higher than the observed in Hami and Erjinaqi. Among the five stations, the highest $PM_{10}$ dust concentration (at Erjinaqi) reached 5000 μg $m^{-3}$ and the second highest (at Zhurihe) reached 4000 μg $m^{-3}$. For Case II, the comparisons for Hami and Erjinaqi are not as good as those for Case I: dust concentration was somewhat overpredicted and its temporal evolution also differed from the observations. However, the simulations for Zhurihe and Zhangjiakou agree well with the observations.

The simulated dust concentration in Beijing for the two cases was lower than the observations, but their agreement was better for Zhangjiakou (about 200 km away from Beijing). Previous studies (Zheng *et al.*, 2004; Zhang *et al.*, 2007) have shown that the dust which affects Beijing normally first passes through Zhangjiakou. The source regions for the dust which affects Beijing are normally the southern part of Mongolia, Inner Mongolia and Beijing local areas (Zheng *et al.*, 2004). During Case I, strong winds occurred in Beijing and it is likely that local dust emission may have been significant. Our model does not have the capacity to simulate local dust emissions, given the complicated underlying surface conditions of the Beijing metropolitan and the surrounding areas. This deficiency of the dust model may have contributed to the less successful model simulation for Case 1. For Case II, wind was too weak in Beijing to generate local dust emission (Figure 13). The dust which affected Beijing was transported dust. Still the simulated dust concentration during the night was weaker than observed. The reasons for this need to be investigated further.

## Dust sources and deposition

The hourly model outputs are used to analyse the dust sources and depositions. Figure 15 shows the simulated total dust emission and deposition for the two cases. For Case I, three dust sources are identified, namely, the eastern part

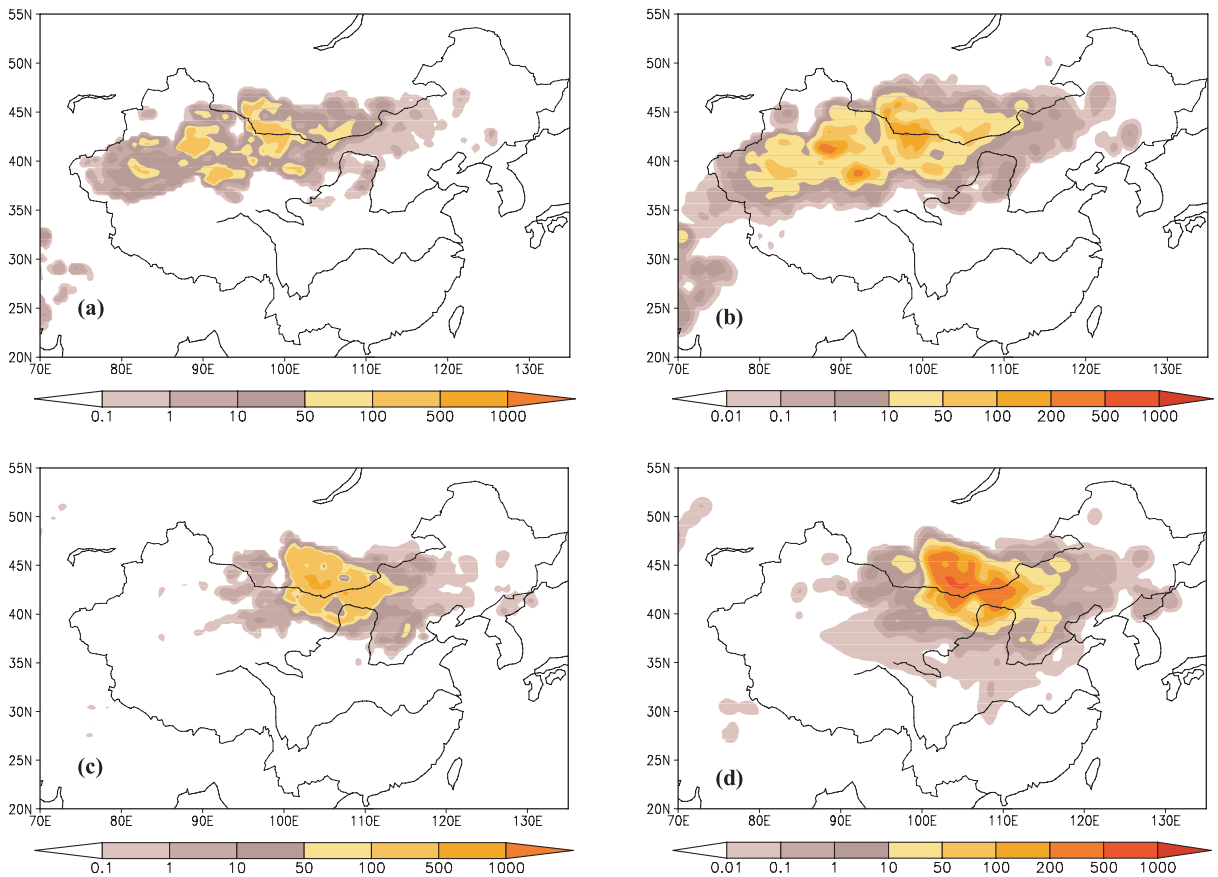


**Figure 15.** The simulated total dust emission (a and c) and total deposition (b and d) in g $m^{-2}$: (a and b) from 0000 UTC 09 April to 0000 UTC 11 April 2006; (c and d) from 0000 UTC 16 April to 0000 UTC 18 April 2006.



DOI: 10.1002/esp

of the Xinjiang Autonomous Region, the southern part of the Xinjiang Autonomous Region (Tarim Basin) and the southern part of Mongolia together with the western part of Inner Mongolia (Figure 15a). In Case 1, dust emission in the Gobi Desert exceeded 50 g $m^{-2}$, but was less than 10 g $m^{-2}$ in the other regions. Deposition occurred over a much wider area, but the areas of strong deposition were the dust-source and the surrounding regions (Figure 15b). During Case I, dust deposition also occurred over Pakistan and north India.

For Case II, the main dust source regions are southern Mongolia, western Inner Mongolia and Gansu (Figure 15c). The strongest emission (over 10 g $m^{-2}$) occurred in the Gobi Desert. Deposition occurred over Mongolia and northern China. The deposition in Beijing and the surrounding areas was about 10 g $m^{-2}$ (Figure 15d). In Case I, dust also affected northwestern China and South Asia, whereas in Case II, dust did not affect those areas.

## Conclusions

In this paper, we have described the main features of northeast Asian dust storms that occurred in Spring 2006, and have used IAPS2.0, an integrated dust storm modelling system, to simulate two of these storms. The main conclusions are as follows:

- The frequency of dust storms in spring 2006 is the highest since 2000.
- Five severe dust storms and six dust storms were reported.
- Weak dust events occurred almost every day from 10 March to middle April.
- The highest frequency of strong dust storms occurred in Inner Mongolia and the Tarim Basin.
- Weaker dust events are more frequent and affect a much wider area.

The severe dust events of 9–11 April (Case I) and 16–17 April (Case II) were selected for the simulation. For these two cases, the pattern and evolution of the simulated and observed dust storms are in general agreement. The simulation of Case II appears to be less successful than the simulation of Case I.

For Case I, the observed and simulated $PM_{10}$ values are in good agreement for the four stations of Hami, Erjinaqi, Zhurihe and Zhangjiakou, although the peak values appear to be overpredicted. The highest value of dust concentration among the five stations is observed in Erjinaqi (Inner Mongolia) with $PM_{10}$ reaching 5000 μg $m^{-3}$. The model has been able to successfully reproduce the airflow patterns in the Tarim Basin, which are complicated by the topography. In Case I, dust emission in the Tarim Basin was mainly caused by the northeasterly wind that originated from the inflow through the east inlet and the downslope flow over the Tianshan Mountains. A vertical circulation, forced by the topography, exists over the Tarim Basin. The dust emitted from the basin is found to converge first to the northern rim of the Tibetan Plateau. There, dust is further transported upward and then northward by a southerly wind in the middle troposphere.

For Case II, dust mainly affected the northeastern part of China. The simulations for Zhurihe and Zhangjiakou agree well with the $PM_{10}$ observations. Because the surface wind is weak, the strong southwesterly in the warm sector of the cyclone transported dust eastward in the lower and middle troposphere. The observed strong deposition in Beijing can be attributed to a low-level inversion, a downward motion and the slow movement of the weather system.

For Case I, dust emission from the Gobi Desert has been found to exceed 50 g $m^{-2}$, but less than 10 g $m^{-2}$ in the other regions of northern China. For Case II, dust emission was confined to a much smaller region. During Case II, strong deposition occurred in Mongolia and in the northern part of China. The deposition in Beijing and its surrounding area has been found to be about 10 g $m^{-2}$. In addition to the Gobi Desert, the dust source regions in the Tarim Basin, the Badain Jaran Desert, Tengger Desert and Hunshandake Sandy Land (Inner Mongolia) also appear to be significant.

### Acknowledgements

The satellite images and the GIS database are provided by the National Satellite Meteorological Center and the Institute of Geographical Sciences and Natural Resources Research, Chinese Academy of Sciences, respectively. This research was supported by supported by the Knowledge Innovation Program of Chinese Academy of Sciences under the Grant No. kzcx2-yw-202 and the National Natural Science Foundation of China under the Grant No. 40875021 and 40620120437.

## References

Chen F, Dudhia J. 2001a. Coupling an advanced land surface–hydrology model with the Penn State–NCAR MM5 modeling system. Part I: model implementation and sensitivity. *Monthly Weather Reviews* **129**: 569–585.

Chen F, Dudhia J. 2001b. Coupling an advanced land surface-hydrology model with the Penn State–NCAR MM5 modeling system, Part II: preliminary model validation. *Monthly Weather Reviews* **129**: 587–604.

Chen F, Mitchell K, Schaake J *et al.* 1996. Modeling of land-surface evaporation by four schemes and comparison with FIFE observations. *Journal of Geophysical Research* **101**(D3): 7251–7268.

Chen F, Janjić Z, Mitchell KE. 1997. Impact of atmospheric surface-layer parameterizations in the new land-surface scheme of the NCEP mesoscale Eta model. *Boundary-Layer Meteorology* **85**: 391– 421.

Gong SL, Zhang XY, Zhao TL, McKendry IG, Jaffe DA, Lu NM. 2003. Characterization of soil dust aerosol in China and its transport and distribution during 2001 ACE-Asia. 2. Model simulation and validation. *Journal of Geophysical Research* **108**: 4262. DOI: 10.1029/2002JD002633

Grell GA, Kuo Y-H, Pasch RJ. 1991. Semi-prognostic tests of cumulus parameterization schemes in the middle latitudes. *Monthly Weather Reviews* **119**: 5–31.

Grell G, Dudhia J, Stauffer D. 1994. *A Description of the Fifth-generation Penn State/NCAR Mesoscale Model (MM5)*. Technical Note NCAR/TN-398+STR, National Center for Atmospheric Research: BOULDER, CO; 117 pp.

Hong S-Y, Pan H-L. 1996. Nonlocal boundary layer vertical diffusion in a medium range forecast model. *Monthly Weather Reviews* **124**: 2322–2339.

Jacquemin B, Noilhan J. 1990. Sensitivity study and validation of a land surface parameterization using the HAPEX-MOBILHY dataset. *Boundary-Layer Meteorology* **52**: 93–134.

Koren V, Schaake JC, Mitchell KE *et al.* 1999. A parameterization of snow pack and frozen ground intended for NCEP weather and climate models. *Journal of Geophysical Research* **104**(D16): 19569–19585.

Lei Hang, Lin Zhaohui, Sun Jianhua, 2005. An improved dust storm prediction system and its simulation experiments. *Climate and Environmental Research* **10**(3): 669–683. (In Chinese with English abstract.)

Lunardini VJ. 1981. *Heat Transfer in Cold Climates*. Van Nostrand Reinhold: New York; 731 pp.

Mahrt L, Ek M. 1984. The influence of atmospheric stability on potential evaporation. *Journal of Climate and Applied Meteorology* **23**: 222–234.

Mahrt L, Pan H-L. 1984. A two-layer model of soil hydrology. *Boundary-Layer Meteorology* **29**: 1–20.

Marticorena B, Bergametti G. 1995. Modeling the atmospheric dust cycle. 1. Design of a soil-derived dust emission scheme. *Journal of Geophysical Research* **100**: 16415–16430.

Marticorena B, Bergametti G, Aumont B *et al.* 1997. Modeling the atmospheric dust cycle. 2. Simulation of Saharan dust sources. *Journal of Geophysical Research* **102D**(40): 4387– 4404.

Pan H-L, Mahrt L. 1987. Interaction between soil hydrology and boundary layer developments. *Boundary-layer Meteorology* **38**: 185–202.

Papayannis A, Zhang HQ, Amiridis V *et al.* 2007. Extraordinary dust event over Beijing, China, during April 2006: Lidar, Sun photometric, satellite observations and model validation. *Geophysical Research Letter* **34**: L07806. DOI: 10.1029/2006GL029125

Peters-Lidard CD, Blackburn E, Liang X, Wood EF. 1998. The effect of soil thermal conductivity parameterization on surface energy fluxes and temperatures. *Journal of Atmospheric Science* **55**: 1209–1224.

Reisner J, Bruintjes RT, Rasmussen RJ. 1998. Explicit forecasting of supercooled water in winter stroms using the MM5 mesoscale model. *Quarterly Journal of the Royal Meteorological Society* **124B**: 1071–1107.

Robinson DA, Kukla G. 1985. Maximum surface albedo of seasonally snow covered lands in the Northern Hemisphere. *Journal of Climate and Applied Meteorology* **24**: 402–411.

Seino N, Sasaki H, Yamamoto A *et al.* 2005. Numerical simulation of mesoscale circulations in the Tarim Basin associated with dust events. *Journal of the Meteorological Society, Japan* **83A**: 205–218.

Shao Y. 2001. A model for mineral dust emission. *Journal of Geophysical Research* **106**: 20239–20254.

Shao Y. 2004. Simplification of a dust emission scheme and comparison with data. *Journal of Geophysical Research* **109**: D10202. DOI: 10.1029/2003JD004372

Shao Y, Dong CH. 2006. A review on East Asian dust storm climate, modeling and monitoring. *Global and Planetary Change* **52**: 1–22. DOI: 10.1016

Shao Y, Leslie LM. 1997. Wind erosion prediction over Australian continent. *Journal of Geophysical Research* **102**: 30091–30105.

Shao Y, Wang JJ. 2003. A climatology of Northeast Asian dust events. *Meteorologische Zeitschrift* **12**(4): 187–196.

Shao Y, Raupach MR, Leys JF. 1996. A model for predicting Aeolian sand drift and dust entrainment on scales from paddock to region. *Austrian Journal of Soil Research* **34**: 309–342.

Shao Y, Jung E, Leslie LM. 2002. Numerical prediction of northeast Asian dust storms using an integrated wind erosion modeling system. *Journal of Geophysical Research* **107**(D24): 4814. DOI: 10.1029/2001JD001493

Shao Y, Yang Y, Wang JJ *et al.* 2003. Northeast Asian dust storms: real-time numerical prediction and validation. *Journal of Geophysical Research* **108**(D22): 4691. DOI: 10.1029/2003JD003667

Sun Jianhua, Zhao Linna, Zhao Sixiong. 2003. An integrated modeling system of dust storm suitable to North China and applications. *Climate and Environmental Research* **8**(2): 125–142. (In Chinese with English abstract.)

Sun Jianhua, Zhao Linna, Zhao Sixiong, Zhang Renjian. 2006. An integrated dust storm prediction system suitable for East Asia and its simulation results. *Global and Planetary Change* **52**: 71–87. DOI: 10.1016

Uno I, Amano H, Emori S, Kinoshita K, Matsui I, Sugimoto N. 2001. Trans-Pacific yellow sand transport observed in April 1998: a numerical simulation. *Journal of Geophysical Research* **106**: 18331–18344.

Wang Z, Ueda H, Huang M. 2000. A deflation module for use in modeling long-range transport of yellow sand over east Asia. *Journal of Geophysical Research* **105**: 26947–26957.

Zhang P, Lu NM, Hu XQ *et al.* 2006. Identification and physical retrieval of dust storm using three MODIS thermal IR channels. *Global and Planetary Change* **52**: 207–215. DOI: 10.1016

Zhang ZG, Gao QX, Jiao MY. 2007. Analysis on source location sand transportation paths of sand dusts affecting Beijing. *Research in Environmental Science* **20**(4): 22–27. (In Chinese with English abstract.)

Zhao LN, Zhao SX. 2006. Diagnosis and simulation of a rapidly developing cyclone related to a severe dust storm in East Asia. *Global and Planetary Change* **52**: 105–120.

Zheng XJ, Yang YW, Yun L. 2004. Some characteristics of dust storm weather affecting Beijing. *Climate and Environmental Research* **9**(1): 14 –23. (In Chinese with English abstract.)

Zhou Zijiang, Wang Xiwen, Niu Ruoyun. 2002. Climate characteristics of sandstorm in China in recent 47 years. *Q. J. Appl. Met.* **13**(2): 193–200. (In Chinese with English abstract.)